

MULTI-PHENOMENA MODELING OF THE NEW BULLET CLUSTER, ZWCL008.8+52, USING *N*-BODY/HYDRODYNAMICAL SIMULATIONS

S. M. MOLNAR¹ AND T. BROADHURST^{2,3}

Draft version September 20, 2021

ABSTRACT

We use hydrodynamical/*N*-body simulations to interpret the newly discovered Bullet-cluster-like merging cluster, ZwCl 0008.8+5215 (ZwCl008 hereafter), where a dramatic collision is apparent from multi-wavelength observations. We have been able to find a self-consistent solution for the radio, X-ray, and lensing phenomena by projecting an off-axis, binary cluster encounter viewed just after first core passage. A pair radio relics traces well the leading and trailing shock fronts that our simulation predict, providing constraints on the collision parameters. We can also account for the observed distinctive comet-like X-ray morphology and the positions of the X-ray peaks relative to the two lensing mass centroids and the two shock front locations. Relative to the Bullet cluster, the total mass is about 70% lower, $1.2 \pm 0.1 \times 10^{15} M_{\odot}$, with a correspondingly lower infall velocity, $1800 \pm 300 \text{ km s}^{-1}$, and an impact parameter of $400 \pm 100 \text{ kpc}$. As a result, the gas component of the infalling cluster is not trailing significantly behind the associated dark matter as in the case of the Bullet cluster. The degree of agreement we find between all the observables provides strong evidence that dark matter is effectively collisionless on large scales calling into question other claims and theories that advocate modified gravity.

Subject headings: galaxies: clusters: general – galaxies: clusters: individual (ZwCl 0008.8+5215) – methods: numerical

1. INTRODUCTION

The Bullet cluster has provided particularly direct evidence for the existence of dark matter by displaying a large offset between the the gas component, marked by X-ray emission, and dark matter traced by gravitationally lensed images (Markevitch et al. 2002). This merging cluster also demonstrates that dark matter is collisionless to high precision, because, although the X-ray shocks unambiguously reveal that two clusters have clearly just collided (Markevitch 2005), the two dark matter centroids are still centered on their respective galaxy members (Clowe *et al.* 2006). When two clusters suffer gravitational encounters their respective member galaxies being relatively small are unlikely to collide with each other. Therefore the cluster member galaxies are effectively collisionless, hence, If the dark matter has an associated collisional cross section it may be revealed by a relative displacement between the two dark matter lensing centroids and their respective member galaxy distributions. The amplitude of this displacement is proportional to the self-interaction cross section of dark matter particles. Using this property, the Bullet cluster was also the first to be used to put upper limits on the self-interaction cross section of dark matter particles providing quantitative evidence that the dark matter is collisionless (Markevitch et al. 2004).

Since the discovery of the Bullet cluster, more merging clusters have been found with offset between the centroids of the intra-cluster gas and the dark matter (MACS J1149.5+2223: Golovich et al. 2016 ; CL0152-1357: Molnar et al. 2012 DLSC J0916.2+2951: Dawson et al. 2012; ACT-CL J01024915: Menanteau et al. 2012; MACS

J0717.5+3745: (Mroczkowski et al. 2012) Mroczkowski et al. 2012; A1758N: Ragozzine et al. 2012; A2744: Merten et al. 2011 A2163: Okabe et al. 2011; ZwCL0008.8+5215: van Weeren et al. 2011; CL0152-1357: Massardi et al. 2010; A1240: Barrena et al. 2009; MACS J0025.4-1222: Bradač et al. 2008; A520: Mahdavi et al. 2007; Bullet Cluster: Clowe et al. 2004)

The collisions of massive clusters of galaxies provide a unique possibility to study the nature of dark matter as these collisions are the most energetic of all phenomena (after the Big Bang) with the power to separate the collisional gas from the confining dark matter gravitational potential, including the galaxies, which provide an effectively collisionless tracer population. Any significant inconsistencies in accounting for the relative dynamics of the components would therefore be of fundamental importance. To examine this possibility to the fullest requires, of course, appropriate simulations that incorporate dark matter and gas. The first test to make in this respect is to compare the best data with collisionless dark matter, which is well described by *N*-body simulations together with an appropriate hydrodynamical numerical scheme for the associated hot gas. The gas is much harder to model, but several high quality codes have been constructed and tested for this purpose with different levels of approximation and numerical schemes – ranging from adaptive mesh refinement (AMR) to smooth particle hydrodynamics (SPH) – and applied to the Bullet cluster (Lage & Farrar 2014; Mastropietro & Burkert 2008; Springel & Farrar 2007); the Sausage cluster (CIZA J2242.8+5301; Molnar & Broadhurst 2017; Donnert et al. 2017) El Gordo (ACT-CT J0102-4915; Zhang et al. 2015; Molnar & Broadhurst 2015); A1758N (Machado et al. 2015); A1750 (Molnar et al. 2013a); and CL0152-1357 (Molnar et al. 2012); for a review see Molnar 2016.

Several examples of extreme collisions have now been analyzed in detail for which the speed of the infalling cluster exceeds the sound speed of the gas, thus merging shocks

¹ Institute of Astronomy and Astrophysics, Academia Sinica, P. O. Box 23-141, Taipei 10617, Taiwan

² Department of Theoretical Physics, University of the Basque Country, Bilbao 48080, Spain

³ Ikerbasque, Basque Foundation for Science, Alameda Urquijo, 36-5 Plaza Bizkaia 48011, Bilbao, Spain

are generated. These shock fronts, in some systems, are traced by radio “relics”, large-scale diffuse synchrotron emission (Enßlin 1999; for a recent review see Feretti *et al.* 2012). There are also very bright gas features corresponding compressed gas that, although subsonic, are relatively dense so that the X-ray emission is enhanced showing a large scale cometary morphology, such as El Gordo (Menanteau *et al.* 2012). This morphology has been readily explained as an off axis binary collision in self-consistent N -body/hydrodynamical numerical simulations assuming zero self-interacting cross section for the dark matter (Zhang *et al.* 2015; Molnar & Broadhurst 2015). Radio relics in El Gordo delineate a bow shock and a back shock. We define bow shock as the shock front in the gas of the main cluster generated by the infalling cluster, which resembles a bow shock of a bullet flying through air. The back shock is the shock front propagating in the gas of the infalling cluster in the opposite direction to the cluster. The back shock was detected by X-ray and SZ observations (Botteon *et al.* 2016; Basu *et al.* 2016). Another such example is the Sausage cluster (CIZA J2242.8+5301), in which, in addition to tidally compressed gas between the two merging clusters highlighted by X-ray emission, there are impressive radio “relics” marking the location of the bow shock front in particular with evidence of a back shock in the radio observations (Molnar & Broadhurst 2017; van Weeren *et al.* 2010).

These simulations are demanding in time and analysis despite the inherent simplicity of binary encounters, because the gas interactions must be resolved well spatially and temporally, and there is a wide range of masses and impact parameters to explore and projection angles involved. With some intuition in exploring the output of these models and the improvements in data quality, we can become more efficient by narrowing the ranges of the relevant initial conditions.

This numerical work has, in the above cases, found consistency with the collisionless dark matter hypothesis by finding compelling agreement among the independent observables including the lensing, radio relic, X-ray and SZ data that are increasingly being obtained for examining the binary collision clusters. A discrepancy that has been advanced for the “Pandora” cluster (A2744) in terms of dark matter offsets is not so readily modeled as the system this multi-model in complexity (Lam *et al.* 2014; Zitrin *et al.* 2014; Merten *et al.* 2011), so such statements are qualitative at present. Further clarification would also benefit from a deeper weak lensing analysis (Medezinski *et al.* 2016). Even for binary collisions it is very clear that approximate or misleading eyeball statements regarding the basic collision parameters are often easily cleared up uniquely, thanks to comparison with the numerical calculations. In particular, statements regarding the relative impact velocity and the time after first core passage at which the system is being viewed are often highly uncertain without the guidance of a full self-consistent simulation (e.g. Golovich *et al.* 2016; Ng *et al.* 2015).

The issue of the relative velocity is particularly interesting as it provides a definitive test of the Λ CDM scenario. The distribution of dark matter halo relative velocities has been calculated in detail by several N -body simulations based on Λ CDM (e.g., Bouillot *et al.* 2015; Thompson & Nagamine 2012), as well as including approximate hydro interactions (Cai *et al.* 2009). The first such consistency test was inspired by the Bullet cluster. The infall velocities in the Bullet cluster, $\sim 3000 \text{ km s}^{-1}$, derived using detailed N -body/hydro-

dynamical simulations based on multifrequency observations seemed to be too high for Λ CDM models (Mastropietro & Burkert 2008; Springel & Farrar 2007). Analyzing large cosmological numerical simulations, Lee & Komatsu (2010) and Thompson & Nagamine (2012) found that the Bullet cluster is incompatible with Λ CDM models. Bouillot *et al.* (2015) arrived at the same conclusion adopting a new halo finder algorithm, ROCKSTAR, and using extreme value statistics. In contrast, Watson *et al.* (2014) and Lage & Farrar (2015) using different cosmological simulations concluded that the Bullet cluster is not excluded by the Λ CDM. Kraljic & Sarkar (2015), using the “Dark Sky Simulations”, the ROCKSTAR algorithm, and extreme value statistics, found that the number of Bullet-cluster-like massive halos is ~ 0.1 , i.e., the Bullet cluster is compatible with the Λ CDM models. However, more high-infall velocity merging clusters have been identified recently (Abell 2744: Owers *et al.* 2011; CL J0152-1347: Molnar *et al.* 2012; MACS J0717.5+3745: Ma, Ebeling & Barrett 2009 and Sayers *et al.* 2013; El Gordo: Molnar & Broadhurst 2015).

The probability to find all of these massive systems simultaneously based on cosmological simulations of Λ CDM models has not been assessed yet. It is an open question today whether their infall velocities are compatible with the predictions of our standard Λ CDM models. Clearly, a statistical sample of such clusters is of great interest to clarify this question further. A confirmation of a sample of merging clusters with high infall velocities could be a serious challenge to the standard Λ CDM models (e.g., Molnar 2015; Kraljic & Sarkar 2015).

Here we apply our well-tested *FLASH* based 3-dimensional (3D) Hydro/ N -body code to a recently discovered Bullet-cluster-like binary collision encounter that has been recently recognized (Golovich *et al.* 2016), but for which self-consistent simulations have yet not been applied. This system has the advantage of showing a clear cut pair of radio relics, a distinct bullet like X-ray morphology, weak gravitation lensing based mass centroids for the two interacting components, and line of sight redshift information for cluster member galaxies (Golovich *et al.* 2016). We follow the time evolution of the merging shocks until they run out of the intra-cluster gas, and test the assumption of collisionless dark matter inherent to the standard LCDM cosmology. We make use of the AMR code, *FLASH* allowing us to follow the shocks in the low density intracluster gas, that is not well represented in the fixed grid Eulerian scheme and codes based on SPH (for a comparison between AMR and SPH simulations see, e.g., Mitchell *et al.* 2009; Agertz *et al.* 2007).

The structure of this paper is as follows. In Section 2 we summarize results from previous analyses of ZwCl008 based on multifrequency observations and numerical simulations. We describe our simulation setup for modeling of ZwCl008 as a binary merger in Section 3. Section 4 presents our results, a dynamical model for ZwCl008, a discussion on the dynamics of merging shocks in clusters similar to ZwCl008, and a comparison with the Bullet cluster. Section 5 contains our conclusions. We adopt a spatially flat Λ CDM cosmology with $h = 0.7$, $\Omega_m = 0.3$, thus $\Omega_\Lambda = 0.7$. Unless stated otherwise, the quoted errors represent 68% Confidence levels (CLs).

2. ZwCl008: THE NEWLY DISCOVERED BULLET-LIKE CLUSTER

The merging cluster ZwCl008, at a redshift of 0.1032, was observed by van Weeren *et al.* (2011) using the Giant-Meterwave Radio Telescope (GMRT) at 241 and 640 MHz and the Westerbork Synthesis Radio Telescope (WSRT) at

1.3-1.7 GHz. They found two radio relics to the east and west from the X-ray peak emission, with the eastern relic much more elongated (first panel in Figure 1). The spectral indices of both relics are steepening towards the cluster center, suggesting that they are moving outward, away from the center of the merging system. The spectral indices at the front of the east and west relics were reported to be -1.2 ± 0.2 and -1.0 ± 0.15 . Adopting these as the spectral indices of the injection distribution, they derive Mach numbers $\mathcal{M} = 2.2_{-0.1}^{+0.2}$ and $\mathcal{M} = 2.4_{-0.2}^{+0.4}$ for the east and west relics; the polarizations were constrained to 5%-25% and 5%-10%.

More recently Kierdorf et al. (2017) carried out high-frequency radio observations of ZwCl008 at 4.85 and 8.35 GHz with the Effelsberg telescope. They found a polarization fraction of the eastern relic between 20% and 30%, and derived a Mach number of $\mathcal{M} = 2.35 \pm 0.1$, in agreement with previous radio measurements of van Weeren et al. (2011).

Most recently, Golovich et al. (2017) carried out a dynamical analysis of ZwCl008 based on detailed radio (JVLA), optical (HST, Subaru/SuprimeCam, Keck/DEIMOS) and X-ray (Chandra/ACIS-I) observations and weak lensing observations (Subaru/HST) to estimate masses of $M_{200,1} = 5.73_{-1.81}^{+2.75} \times 10^{14} M_{\odot}$ and $M_{200,2} = 1.21_{-0.63}^{+1.43} \times 10^{14} M_{\odot}$ for the main and infalling cluster respectively, which is a mass ratio of $\simeq 5$.

Golovich et al. (2017) used this information as input in their dynamical model, which is based on fixed NFW (Navarro, Frenk & White 1997) gravitational potentials for the two components and zero impact parameter, ignoring the effects of gas, gravitational tidal effects, mass loss, and integrating the equations of motion numerically. Golovich et al. estimated the merger velocity at pericenter, V_p , and obtained $V_p = 1800_{-300}^{+400} \text{ km s}^{-1}$. The inclination angle relative to the plane of the sky, θ , was constrained to $6.6^{\circ} \lesssim \theta \lesssim 31^{\circ}$, which is consistent with the direct constraint derived from radio polarization measurements: $\theta \lesssim 40^{\circ}$. Golovich et al. concluded that the gas of the two merging subclusters is still moving outward, and derived the phase of the system as either $0.76_{-0.27}^{+0.24}$ Gyr or $1.3_{-0.35}^{+0.90}$ Gyr after the first core passage for the outgoing phase and infalling phase (after the turnover) respectively. They could not distinguish between the outgoing and returning phase because their model is time symmetric, includes only the dark matter and not gas, hence the X-ray emission, which provides information of the gas, could not be interpreted.

3. MODELING ZwCl008 USING HYDRODYNAMICAL SIMULATIONS

Our main goals were to obtain a reasonable physical model for the newly discovered Bullet-cluster-like merging cluster, ZwCl008, using N -body/hydrodynamical simulations, and thus estimate the infall velocity and constrain the phase of the collision with high precision. We have not carried out a systematic search for all the initial parameters and determined their errors with statistical measures, which would require many more simulations. The errors we quote for the results from our simulations are conservatively estimated.

3.1. Details of the simulations

We modeled ZwCl008 in 3D using an Eulerian N -body/hydrodynamic code *FLASH* (developed at the Center for Astrophysical Thermonuclear Flashes at the University of Chicago; Fryxell et al. 2000; Ricker 2008). *FLASH* is a publicly available AMR code, which can be run in paral-

TABLE 1
IDS AND INPUT PARAMETERS FOR DIFFERENT MODELS USED IN OUR HYDRODYNAMICAL SIMULATIONS.

ID ^a	M_{vir1} ^b	c_{vir1} ^b	M_{vir2} ^c	c_{vir2} ^c	P ^d	V_{in} ^e
P400V18B	7.0	6	5.0	8	400	1800
P100V15G	6.0	6	1.5	8	100	1500
P300V18	7.0	6	5.0	8	300	1800
P500V18	7.0	6	5.0	8	500	1800
P400V18M1	7.0	6	5.5	8	400	1800
P400V18M2	7.0	6	4.5	8	400	1800
P400V18M3	7.5	6	5.5	8	400	1800
P400V18M4	7.5	6	5.0	8	400	1800
P400V18M5	7.5	6	4.5	8	400	1800
P400V18M6	6.5	6	5.5	8	400	1800
P400V18M7	6.5	6	5.0	8	400	1800
P400V18M8	6.5	6	4.5	8	400	1800
P400V15	7.0	6	5.0	8	400	1500
P400V20	7.0	6	5.0	8	400	2000

^a IDs of the runs indicate the impact parameters in kpc and the infalling velocities in units of 100 km s^{-1}

^b Virial mass in $10^{14} M_{\odot}$ and concentration parameter for the main cluster (1).

^c Virial mass in $10^{14} M_{\odot}$ and concentration parameter for the infalling cluster (2).

^d Impact parameter in units of kpc.

^e Infall velocity of cluster 2 in km s^{-1} .

lel computer architectures. We assumed a binary merger for ZwCl008 and included dark matter and gas self-consistently taking their gravity into account dynamically. We used our well-established method to carry out merging cluster simulations (Molnar & Broadhurst 2017, 2015; Molnar et al. 2013a,b, 2012). For our simulations, we adopted a large box size (13.3 Mpc on a side) to capture the outgoing merger shocks and avoid losing mass during the time we ran our simulations. Our highest resolution, 12.7 kpc was reached at the cluster centers, merger shocks, and in the turbulent regions behind the shocks. We chose 3D Cartesian coordinate system, x, y, z , with the x, y plain containing the centers of the clusters and the initial (relative) velocity vector of the infalling cluster in the positive x direction. We included shock heating, the most important non-adiabatic process in merging clusters, and ignored other heating and cooling processes.

The initial models of the clusters were assumed to have spherical geometry with cut offs of the dark matter and gas density at the virial radius, R_{vir} . We assumed an NFW model (Navarro, Frenk & White 1997) for the dark matter distribution,

$$\rho_{DM}(r) = \frac{\rho_s}{x(r)(1+x(r))^2}; \quad r \leq R_{vir}, \quad (1)$$

where $x(r) = r/r_s$ ($r_s = R_{vir}/c_{vir}$) and ρ_s , are scaling parameters for the radius and the amplitude of the density, and c_{vir} is the concentration parameter. We adopted a non-isothermal β model for the gas density,

$$\rho_{gas}(r) = \frac{\rho_0}{(1+y^2)^{3\beta/2}}; \quad r \leq R_{vir}, \quad (2)$$

where $y = r/r_{core}$, is the scaling parameters for the radius, r (in units of the core radius, r_{core}), and ρ_0 , is the density at the center of the cluster. The exponent, β determines the fall

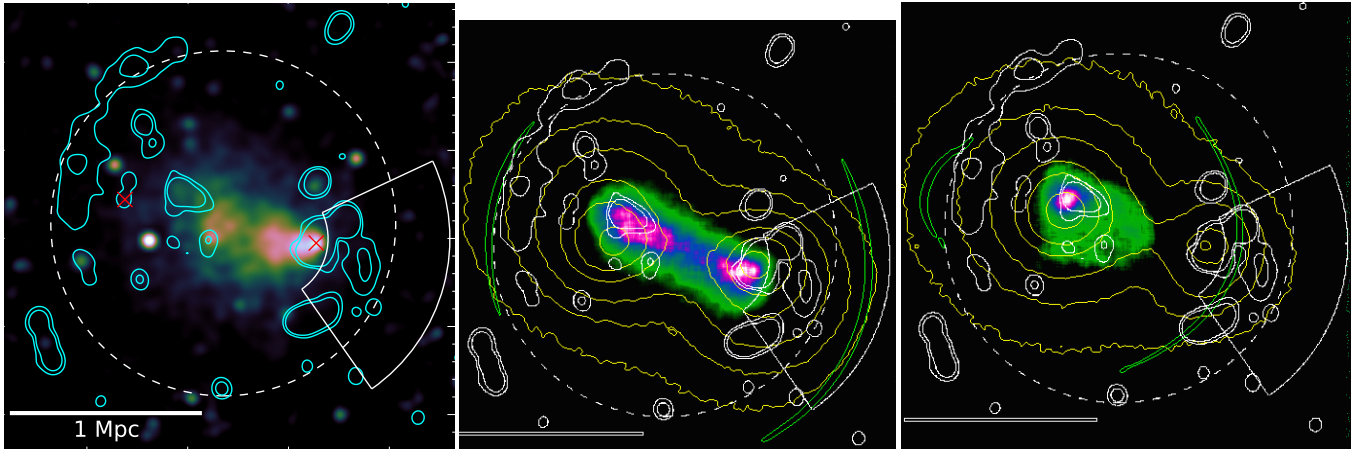


FIG. 1. — 1st panel: *Chandra* X-ray color image of ZwCl008 with the WSRT radio contours (cyan) based on WSRT observations overlaid (from Golovich et al. 2017; van Weeren et al. 2011). The white dashed circle and the horizontal bar represent R_{500} and a length of 1 Mpc. The white annular sector marks the proposed shock region (see Golovich et al. 2017). The two BCGs are shown by red crosses. 2nd panel: On the same scale, simulated X-ray image based on our best model (run P400V18B) at $t = 428$ Myr after the 1st core passage with the contours of the dark matter distribution overlaid (yellow). The green contours represent the outgoing shocks. The viewing angle was chosen to match the observations (see text for details). The bow shock on the right ahead of the infalling cluster moving to the right, the back shock on the left is moving to the left, to the opposite direction to the motion of the infalling cluster. 3rd panel: On the same scale, our run P10V15G with initial conditions suggested by Golovich et al. (2017). There is only one X-ray peak, which is associated with the gas of the main cluster. The gas of the infalling cluster has been stripped off as a result of the relatively large velocity of the infalling cluster and the small impact parameter.

off of the density distribution at large radii. We adopted $\beta = 1$, suggested by cosmological numerical simulations for the large scale distribution of the intracluster gas in equilibrium (excluding the filaments; see Molnar et al. 2010).

We derived the gas temperature as a function of the radius, $T(r)$, assuming hydrostatic equilibrium adopting $\gamma = 5/3$ for the ideal gas equation of state. We used a gas fraction, f_{gas} , $f_{gas} = 0.14$, and represented baryons in galaxies together with the collisionless dark matter particles, since, for our purposes, galaxies can also be considered collisionless.

It is less straightforward to model a stable dark matter density distribution than a gas distribution. The hydrostatic equilibrium assumption provides a stable distribution for the gas, but the dark matter, modeled as particles, has no pressure, interacting only gravitationally with itself and the gas, which means that they move on orbits in the potential of the cluster. We use the local Maxwellian approximation for the amplitude of the velocities of the dark matter particles: we randomly sample a Maxwellian distribution with a velocity dispersion as a function of radius, r , $\sigma_v(r)$ derived from the Jeans equation assuming that the distribution of $\sigma_v(r)$ is isotropic (Łokas & Mamon 2001). We assumed an isotropic distribution for the direction of the velocity vectors (for more details of the set up for our simulations see Molnar et al. 2012).

3.2. FLASH Runs

We have run a series of *FLASH* simulations varying the initial masses, concentration parameters, impact parameter, and infall velocity of our models. Our aim was to find a physical model for ZwCl008 with a reasonable agreement with observations. Our simulations were constrained by the masses and positions of the dark matter centers derived from weak gravitational lensing, X-ray morphology (Golovich et al. 2017), and the positions of the outgoing merging shocks inferred from radio observations (van Weeren et al. 2011). The long bright radio relic to the east most likely marks the location of the back shock, as in the CIZA J2242.8+5301 cluster, as demonstrated by Molnar & Broadhurst 2017), due to the limb brightening of the spherical surface of the relic viewed in projection. The position of the bow shock associated with the in-

falling cluster is much less certain. This forward shock is not detected by the X-ray observations (Golovich et al. 2017)). We estimate from our models that it should lie significantly beyond the small radio relic that we nevertheless do associate with this shock. The reason for this displacement can be simply geometric in origin, because such shock surfaces are convex in shape, thus, in projection, radio relics on their surface may often appear to lie behind the front when viewed from the side despite being generated by the shock (e.g. planetary nebulae appear like a ring, but they are spherical shells). In other words, because radio relics cannot be expected to trace the full shock surface uniformly, but have a patchy covering, thus it is likely to see radio relics appearing “inside” the projected shock front, and only occasionally marking the projected shock itself when a relic happens to cover some of the projected area of the shock front. When that happens, the radio relic can be of high surface brightness as the projected radio emission (which is optically thin) adds up in projection. Indeed, notable examples of large shock fronts of anomalously bright such are known, in particular, the bow shock of CIZA J2242.8+5301 (van Weeren et al. 2011) that modeling has been shown to coincide with their observed projected shock front (Molnar & Broadhurst 2017).

We have carried out a suit of simulations to provide a rough estimate on the errors on the infall velocity, impact parameter, and masses of the merging system before the collision. A systematic parameter search is currently beyond reach of conventional high speed computing resources based on CPUs.

Table 1 contains a list of initial parameters of those simulations we discuss in this paper. This is a narrow subset of parameter space that contains our best solutions with enough spread to illustrate the observable effects of moving away from the best-fit solution. The first column contains the IDs of our runs as $P_{ijk}V_{mn}$, where P_{ijk} is the impact parameter in kpc, and V_{mn} is the infall velocity in units of 100 km s^{-1} . In columns 2 to 5 we show the virial masses (in units of $10^{14} M_{\odot}$) and concentration parameters (c_{vir}) of the two sub-clusters. Columns 6 and 7 contain the impact parameters, P , and infall velocities (V_{in}) in km s^{-1} .

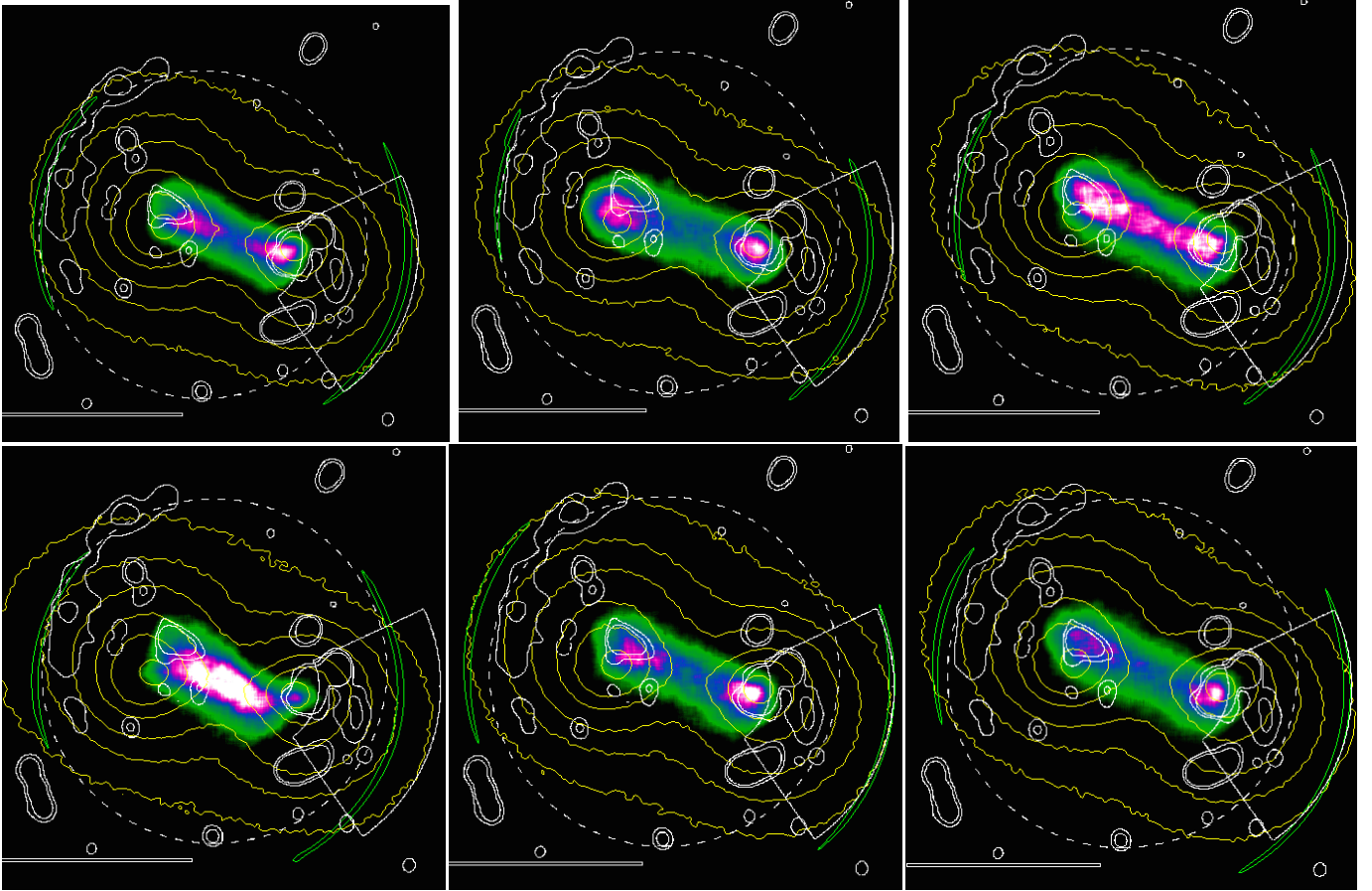


FIG. 2.— Samples of simulations which do not fully resemble the X-ray morphology of ZwCl008. The color code is the same as in the second panel in Figure 1 Left to right: First row: 1st and 2nd panel show runs with $P = 300$ and 500 kpc (P20V18 and P50V18) Second row: 1st and 2nd panel show $V_{in} = 1500$ and 2000 km s^{-1} ; The 3rd panel in the first and second row display the best model, but before and after the best-fit epoch (412 Myr and 444 Myr after the first core passage; run P40V18). The best-fit epoch is $t_{obs} = 428$ Myr after the first core passage. See Table 1 for a list of initial parameters for the runs.

4. RESULTS AND DISCUSSION

4.1. Dynamical Model for ZwCl008

The second panel in Figure 1 shows a simulated X-ray color image of our best-fit model at the epoch of $t_b = 428$ Myr after the first core passage for ZwCl008, run P400V18B with infall velocity, $V_{in} = 1800$ km s^{-1} , impact parameter, $P = 400$ kpc, and masses $M_{vir1} = 7$ and $M_{vir2} = 5 \times 10^{14} M_{\odot}$ (main and infalling cluster). The yellow contours represent the projected dark matter distribution from our simulation. The white contours are based on radio observations, the white dashed circle and the horizontal bar represent R_{500} and a physical length of 1 Mpc (from Golovich et al. 2017; as in the first panel). The viewing (rotation) angles were chosen the following way. First we rotated the system with an angle, $\varphi = 30^{\circ}$ (“roll angle”), around the axis connecting the two dark matter centers (rotation around the y axis) then we rotated this axis with an angle, $\theta = 31^{\circ}$, out of the $x-y$ plane. θ was chosen to provide a projected distance between the two dark matter centers, $D = 940$ kpc, to match the positions of the observed centers based on weak lensing mass reconstruction, the roll angle was chosen to find the best match with the observed X-ray morphology (Golovich et al. 2017). We choose the output (epoch) which could be rotated in a way that the position of the back shock is near the eastern edge of the observed long radio relic in the east of the X-ray peak and the bow shock in the west is not inside the radio relic associated with it, as radio

observations suggest (van Weeren et al. 2011). The shocks in our simulated images were located based on projected pressure gradients. A detailed description of our method to generate mock X-ray and mass surface density images can be found in Molnar & Broadhurst (2015).

In Figure 2, we show images of models for ZwCl008, which do not satisfy our requirements for a good match with the data. In this figure the color images represent the simulated X-ray surface brightness, the color code for the contours is the same as in the second panel in Figure 1. The procedure was the following. First we aligned the position of the X-ray peak associated with the infalling cluster with that of the observed, then we choose the projection angles to match the distances and position angles between the dark matter centers to match those derived from weak lensing observations. In the third step, if it was possible, we selected cases where the position of the back shock is near the eastern edge of the long radio relic in the east of the X-ray peak.

The first and second panels in the first row show runs with only the impact parameters changed to $P = 300$ and 500 kpc (runs P20V18 and P50V18) from the best model (run P400V18 with $P = 400$ kpc). The X-ray morphology of P20V18 (first panel) is too elongated along the line connecting the two dark matter centers. Run P50V18 displays

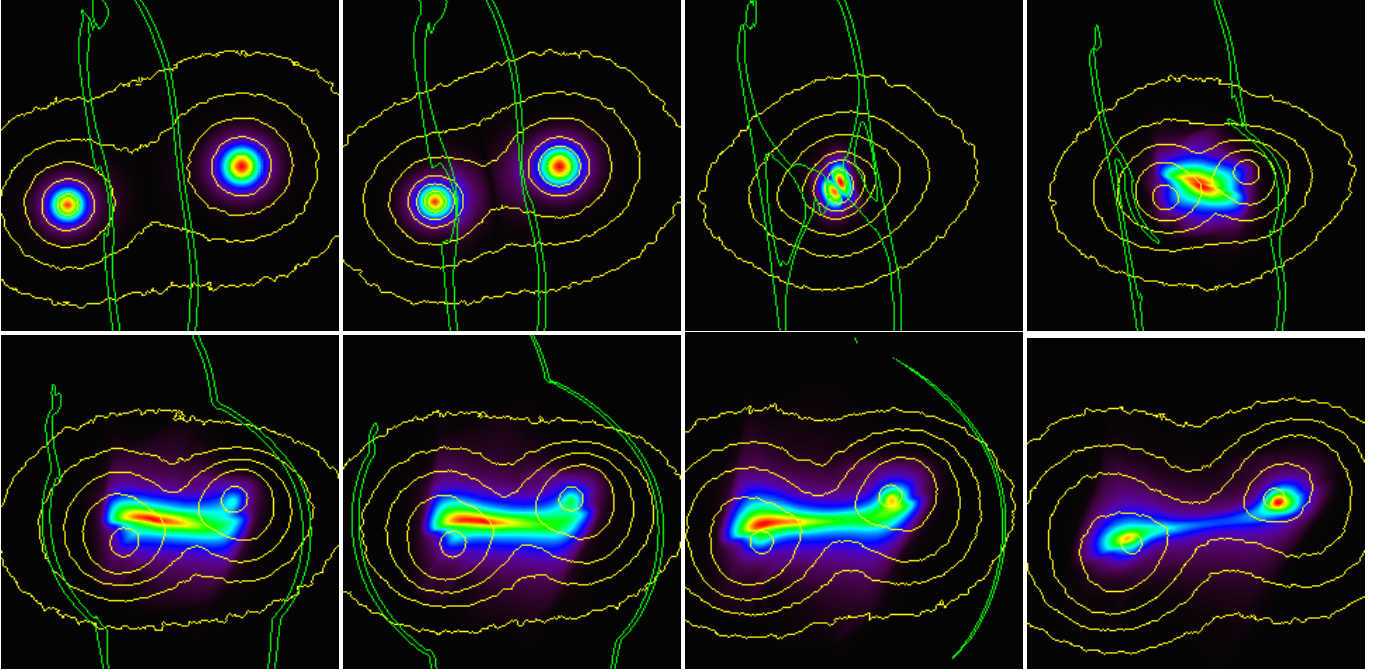


FIG. 3.— Merging shocks and the distribution of the mass surface density of dark matter (green and yellow contours) overlaid on the X-ray emission (color image) as a function of time before and after the first core passage based on our best model for ZwCl008 (run P400V18, see Table 1). We assumed that the collision occurs in the plane of the sky (projections in the LOS). The panels are 3 Mpc on a side. Left to right first and second row the epochs (relative to the first core passage; $t_0 = 0$) are: $t = -475, -317, 0, 238,$ and $t = 396, 459, 555, 713$ Myr. The infalling cluster passes the main cluster from below moving east to west. Panels in the first row: The first two panels in the first row show epochs before the first core passage. The 3rd panel represents the epoch of the first core passage. The two dark matter peaks overlap at the center. The 4th panel shows the phase right after the first core passage. Panels in the second row show phases of the collision when there are two X-ray peaks. The first two panels show two shocks ahead of the cluster centers moving outwards. The 3rd panel shows the phase when the back shock already ran out of the gas of the infalling cluster. The bow shock is still moving outward (towards west). The 4th panel shows a later epoch, when both shocks ran out of the gas of the merging system, and the gas is falling back to the cores of the dark matters of the two components.

two X-ray peaks with large separation and very small offset from the dark matter centers. The first and second panel in the second row show simulations changing only the relative (infall) velocity of the infalling cluster to $V_{in} = 1500$ and 2000 km s^{-1} (runs P40V15 and P40V20) to bracket our best model which $V_{in} = 1800$ km s^{-1} (run P400V18). In the first panel, the very bright X-ray peak is associated to the main cluster, not to the infalling cluster as observed, in the second panel the back shock is farther than observed.

The third panel in the first and second row display the best model but at $t = 412$ Myr and 444 Myr after the first core passage (runs P40V18T1 and P40V18T2), before and after the best-fit epoch. The best-fit epoch is $t_{obs} = 428$ Myr after the first core passage (run P40V18). See Table 1 for a list of initial parameters for the runs. The third panel in the first row shows two bright X-ray peaks with enhanced emission from the tidal bridge between them, which differs from the data where the X-ray peaks have a large brightness ratio and a less enhanced bridge between them. The third panel in the second row shows two X-ray peaks with a large separation and a small offset for both X-ray peaks, again differing significantly with respect to the observed morphology.

We conclude from our suite of N -body/hydrodynamical simulations that ZwCl008 is viewed at about 428 Myr after first core passage, and that the infalling cluster has a mass $M_{vir,2} = 5 \pm 0.5 \times 10^{14} M_{\odot}$ moving to the west, disrupting the gas of the main cluster with mass $M_{vir,1} = 7 \pm 0.5 \times 10^{14} M_{\odot}$, so that it lies to the west of the main cluster at the observed epoch. Our model also clearly confirms that the disrupted gas of the main cluster is offset from its the dark matter center

as the data seem to indicate. Our simulations clearly demonstrate that the merging cluster, ZwCl008, is in the outgoing phase just after the first core passage, before the first turnover. The gas and dark matter associated with the two components are moving outward (the infalling cluster moving to the east, the main cluster to the west; see first and second panels in Figure 1).

These results are in broad qualitative agreement with the results of Golovich et al. (2017), but clearly prefer a recent post collision epoch and exclude their later, post collision epoch option of 1300 Myr, as by then the shock fronts predicted by our model will have long left the system. Also, our best model has significantly larger mass, $1.2 \times 10^{15} M_{\odot}$, and a smaller mass ratio, 1.4 , than those suggested by Golovich et al. ($6.9 \times 10^{14} M_{\odot}$ and 4.75).

We performed a simulation with initial conditions suggested by Golovich et al. (2017) (run P10V15G). We show the result in the third panel in Figure 1. There is only one X-ray peak, which is associated with the gas of the main cluster. We chose a projection, which provides a roughly match to the positions of the two merger shocks with those observed. However, there is no X-ray peak associated with the infalling cluster, contrary to the observations. The gas of the infalling cluster has been stripped off as a result of the relatively large velocity of the infalling cluster (1500 km s^{-1}) and the small impact parameter (100 kpc). Note, that Golovich et al. (2017) assumed zero impact parameter, which would make it even easier to strip all the gas from the infalling cluster. We chose a finite, but small impact parameter since the observed X-ray morphology is not symmetric.

4.2. Outgoing Merging Shocks in ZwCl008

The properties of merging shocks were studied in detail by making use of N -body/hydrodynamical simulations (e.g., Molnar & Broadhurst 2017; Ha et al. 2017). In this section we study the evolution of merging shocks as a function of time around the first core passage before the first turnover using our best solution for ZwCl008 as an example.

The evolution of merging shocks is illustrated in Figure 3. The panels in this figure show a color image of the X-ray emission with contours of the dark matter distribution (yellow) and the merging shocks (green) superimposed. We used a projection along the z axis, i.e., we assumed that z coincides with the line of sight (LOS), and the collision takes place in the plane of the sky (x, y plane). The infalling cluster passes the main cluster center from below moving east to west (second panel in the first row; run P40V18). The time is measured in Myr relative to the first core passage ($t_0 = 0$ Myr; left to right first: $t = -475, -317, 0, 238$, Myr, and second row: $t = 396, 459, 555, 713$ Myr).

The first two panels in the first row show epochs before the first core passage, when only the outer regions of the gas in the two clusters collide. The shocks move ahead of the two clusters generating them in the same direction as their respective dark matter (the shock on the east moves to west, the shock on the west moves to east). The third panel represents the epoch of the first core passage. The two dark matter peaks overlap at the center; they are slightly ahead of the X-ray peaks. The structure of the merging shocks change, multiple shocks are generated due to the collision of the more dense gas in the merging clusters. The fourth panel shows a phase right after the first core passage, when there is only one X-ray peak and the bow shock on the west in the gas of the main cluster is moving to the west ahead of the infalling cluster. The back shock in the east propagates to the east in the gas of the infalling cluster. Panels in the second row show phases after the first core passage, when there are two X-ray peaks. The first two panels show two shocks ahead of the cluster centers moving outward. The third panel shows a phase when the back shock already ran out of the gas of the infalling cluster. The bow shock is still moving outward (towards west). The fourth panel shows a later epoch, when both shocks ran out of the gas of the merging system, and the gas is falling back to the cores of the dark matter of the two components.

We study these outgoing merging shocks in detail because of their importance in determining the dynamical state of the merging cluster, and the phase of the collision. The phase of the collision is important for particle acceleration models, because the physical properties of the shock depend on it, and these properties have a large impact on particle acceleration (e.g., Fujita et al. 2016; Kang & Ryu 2016; Stroe et al. 2014), as well as testing cosmological models (e.g. Molnar 2015).

The reason why the outgoing shocks constrain the phase of the collision well right after the first core passage in the outgoing phase is that they move fast and run out of the gas as they propagate with a high speed in the low density gas at the outskirts of the system. Because of these relatively high outer shock speeds, these shocks can (re)accelerate particles and generate luminous radio relics for a limited time. As a consequence shocks and bright relics can only be expected to be detected in a pair of merging clusters relatively soon after the first core passage, before the first turnaround, after which the relics become fainter without a shock to provide additional energy.

In general, as we see here, if the observed shocks were to lie in between the two X-ray peaks associated with relaxed cluster centers, then we would conclude that the merging system is being viewed before the first core passage, as shown in the first panel in Figure 3, such as the case of, e.g., Abell 1750 (Molnar et al. 2013a). Disturbed X-ray morphology displaying with one or two X-ray peaks within one or two shocks instead suggests a system caught after first core passage (e.g., Molnar & Broadhurst 2015; Mastropietro & Burkert 2008).

Figure 3 also illustrates how fast the outgoing shocks propagate in a merging cluster similar to ZwCl008. After ~ 500 Myr, both the bow shock and the back shock propagating in the gas of the main and the infalling cluster ran out of the system (panel 4 in Figure 3). The velocity relative to the ambient gas of the bow shock (the shock on the west moving to west) is 4500 km s^{-1} , the back shock propagates faster (to the east) with 4900 km s^{-1} . At these speeds, the merging shocks (bow and back shocks) would run out of the gas in 470 and 380 Myr after the first core passage, but our numerical simulations suggest that they run out in 618 and 522 Myr. The turnover occurs 1.5 Gyr after the first core passage, thus, well before the turn over, both merger shocks leave the system. This is a general feature of merging shocks more colliding clusters with moderate mass ratios and infall velocities $\gtrsim 1000 \text{ km s}^{-1}$.

We derive the Mach numbers for the merging shocks based on our best model using the temperature jump at the shocks, as it is done using temperature based on X-ray observations. The Rankine-Hugoniot jump conditions provide the connection between the temperature jump, T_2/T_1 , and the Mach number,

$$\frac{T_2}{T_1} = \frac{5\mathcal{M}^2 + 14\mathcal{M}^2 - 3}{16\mathcal{M}^2}, \quad (3)$$

where T_1 and T_2 are the pre- and post-shock temperatures (e.g., Molnar & Broadhurst 2017; Akamatsu et al. 2015; for a review see Markevitch & Vikhlinin 2007). Using the temperature jump from our simulations at the shocks in Equation 3, we obtain Mach numbers for the merging shocks directly from the physical (not the observed) temperature ratios (the bow shock and back shock to the west and east): $\mathcal{M}_{w, \text{simu}} = 5.5$ and $\mathcal{M}_{e, \text{simu}} = 6.5$.

4.3. Comparing ZwCl008 to the Bullet Cluster

It has been suggested that ZwCl008 is an older, less massive version of the Bullet Cluster (Golovich et al. 2016), where the less massive infalling cluster has pushed the gas of the main cluster out of equilibrium and, as a result, the X-ray morphology, which traces the gas of the main cluster, is irregular (X-ray feature in the east in the first panel in Figure 1). However, our hydrodynamical simulations suggest that the cometary-like X-ray peak in ZwCl008 near the center of mass of the smaller western cluster (see first panel in Figure 1) marks the gas density maximum of the infalling cluster, similar to El Gordo (Molnar & Broadhurst 2015), unlike the bullet cluster, in which the wedge-shaped bright X-ray feature marks a contact discontinuity. The shock in the Bullet cluster is a faint X-ray feature ahead of the merging shock to the west (e.g., Markevitch & Vikhlinin 2007). Based on our best model, ZwCl008 is only 428 Myr after the first core passage, and in a much earlier phase than the turnover, 1.5 Gyr, like the Bullet cluster.

Our results suggest instead that, because of a larger impact parameter for the collision in ZwCl008 and the lower infall

velocity relative to the Bullet cluster, the ram pressure cannot fully hold back the gas relative to the dark matter in the infalling cluster, as opposed to the case of the Bullet cluster. Instead, the infalling cluster in ZwCl008 passes relatively unhindered by the gas of the main cluster since it does not penetrate through the central dense gas of the main cluster.

5. CONCLUSIONS

We have performed a set of self-consistent N -body/hydrodynamical simulations based on *FLASH*, a publicly available AMR code, augmenting our existing library of binary cluster encounters generated in our previous work, in order to study the particular dynamics during the collision of the merging cluster ZwCl008. We have modeled ZwCl008 as a binary merger, constraining the initial parameters using gravitational lensing, X-ray morphology and observations of radio relics. Unfortunately the merger shock positions cannot be determined from the *Chandra* observations without longer X-ray exposures. Therefore, we refer to the positions of the pair of opposing distinctively polarized radio relics that we can assume to have resulted from the two predicted outgoing shocks and a simple geometrical argument (see Section 4.1) to limit the current shock locations. The detailed X-ray morphology and the locations of the two lensing centroids were used to constrain the impact parameter and the infall velocity of the collision, as well as the viewing angle.

We have demonstrated, that the outgoing shocks travel fast ($4000\text{-}5000\text{ km s}^{-1}$) in the low density outer gas of the two subclusters, and, therefore, their positions relative to those of the mass peaks can be used to accurately derive the phase of the collision. Thus, merging shocks can (re)accelerate particles and generate relics only for a limited time $\lesssim 5 \times 10^8$ yr, so that shocks and bright relics can be detected in a merging system soon after the first core passage, before the first turnaround. After that time the relics become fainter after no shocks feed them as the electrons loose energy. This point has been unappreciated in earlier work (Golovich et al. 2017; Ng et al. 2015) where later stage merging has been entertained without the guidance of hydrodynamical simulations like those presented in this paper.

Based on our N -body/hydrodynamical simulations, we derive an impact parameter of 400 ± 100 kpc, and an infall velocity of $1800 \pm 300\text{ km s}^{-1}$, with virial masses of $M_{\text{vir},1} = 7 \pm 0.5 \times 10^{14} M_{\odot}$ and $M_{\text{vir},2} = 5 \pm 0.5 \times 10^{14} M_{\odot}$ for the main and infalling cluster respectively. We find that ZwCl008 is

observed about 430 Myr after the first core passage. Our simulations clearly demonstrate that ZwCl008 is currently in the outgoing phase, well before the first turnover, otherwise the forward and reverse shock fronts would have long run out of the system to the east and west.

Our numerical simulations represent the first attempt to model the newly discovered Bullet-cluster-like merging system ZwCl008 using self-consistent N -body/hydrodynamical simulations. Previously ZwCl008 was modeled by Golovich et al. (2017) using their method based on a model assuming fixed NFW profiles for the dark matter distribution for the merging subclusters assuming zero impact parameter and ignoring the gas components (Dawson 2013). However, their model cannot distinguish between phases of outgoing or infalling after the first turnover. Our full self-consistent simulation containing dark matter and gas can constrain the impact parameter, the phase of the collision, and the viewing angle with the location of the merging shocks to provide a both check on the apparent interpretation of this system as a binary encounter and to provide reliable estimates of the basic masses, velocities and the age and orientation of the system.

The degree of agreement we find between all the reliable observables of the binary merging cluster ZwCl008 and those based on our best model derived from N -body/hydrodynamical simulations along with self-consistent simulations of other merging clusters provides further strong evidence that dark matter is effectively collisionless on large scales. These results support the remarkable insight into this question initially gained by the Bullet cluster. This self consistency calls into question other claims and theories that advocate modified gravity, where the aim is to “emulate” dark matter, simply, because the lensing contours indicating the location of the gravitational potential do not follow the dominant baryonic material that is composed of gas. Instead the detailed gas distribution relative to the lensing data indicates the contrary, that dark matter dominates and it is collisionless to within the precision of the data.

The code *FLASH* used in this work was in part developed by the DOE-supported ASC/Alliance Center for Astrophysical Thermonuclear Flashes at the University of Chicago. We thank the Theoretical Institute for Advanced Research in Astrophysics, Academia Sinica, for allowing us to use its high performance computer facility to carry out our simulations.

REFERENCES

- Agertz, O., Moore, B., Stadel, J., et al. 2007, *MNRAS*, 380, 963
 Akamatsu, H., van Weeren, R. J., Ogrean, G. A., et al. 2015, *A&A*, 582, A87
 Barrena, R., Girardi, M., Boschin, W., & Dasí, M. 2009, *A&A*, 503, 357
 Basu, K., Vazza, F., Erler, J., & Sommer, M. 2016, *A&A*, 591, A142
 Botteon, A., Gastaldello, F., Brunetti, G., & Kale, R. 2016, *MNRAS*, 463, 1534
 Bradač, M., Allen, S. W., Treu, T., Ebeling, H., Massey, R., Morris, R. G., von der Linden, A., & Applegate, D. 2008, *ApJ*, 687, 959
 Bouillot, V. R., Alimi, J.-M., Corasaniti, P.-S., & Rasera, Y. 2015, *MNRAS*, 450, 145
 Cai, Y.-C., Angulo, R. E., Baugh, C. M., et al. 2009, *MNRAS*, 395, 1185
 Clowe, D., Bradač, M., Gonzalez, A. H., et al., 2006, *ApJ*, 648, L109
 Clowe, D., Gonzalez, A., & Markevitch, M. 2004, *ApJ*, 604, 596
 Dawson, W. A. 2013, *ApJ*, 772, 131
 Dawson, W. A., et al. 2012, *ApJ*, 747, L42
 Donnert, J. M. F., Beck, A. M., Dolag, K., & Röttgering, H. J. A. 2017, *MNRAS*, 471, 4587
 Enßlin, T. A. 1999, *Diffuse Thermal and Relativistic Plasma in Galaxy Clusters*, 275
 Feretti, L., Giovannini, G., Govoni, F., & Murgia, M., 2012, *A&A Rev.*, 20, 54
 Fryxell, B., et al. 2000, *ApJS*, 131, 273
 Fujita, Y., Akamatsu, H., & Kimura, S. S. 2016, *PASJ*, 68, 34
 Golovich, N., Dawson, W. A., Wittman, D., et al. 2016, *ApJ*, 831, 110
 Golovich, N., van Weeren, R. J., Dawson, W. A., Jee, M. J., & Wittman, D. 2017, *ApJ*, 838, 110
 Ha, J.-H., Ryu, D., & Kang, H. 2017, arXiv:1706.05509
 Hoang, D. N., Shimwell, T. W., Stroe, A., et al. 2017, *MNRAS*, 471, 1107
 Kang, H., & Ryu, D. 2016, *ApJ*, 823, 13
 Kierdorf, M., Beck, R., Hoeft, M., et al. 2017, *A&A*, 600, A18
 Kraljic, D., & Sarkar, S. 2015, *JCAP*, 4, 050
 Lage, C., & Farrar, G. 2014, *ApJ*, 787, 144
 Lage, C., & Farrar, G. R., 2015, *JCAP*, 2, 038
 Lam, D., Broadhurst, T., Diego, J. M., et al. 2014, *ApJ*, 797, 98
 Lee, J., Komatsu, E., 2010, *ApJ*, 718, 60
 Łokas, E. L., & Mamon, G. A. 2001, *MNRAS*, 321, 155
 Ma, C.-J., Ebeling, H., & Barrett, E., 2009, *ApJ*, 693, L56

- Machado, R. E. G., Monteiro-Oliveira, R., Lima Neto, G. B., & Cypriano, E. S. 2015, MNRAS, 451, 3309
- Mahdavi, A., Hoekstra, H., Babul, A., Balam, D. D., & Capak, P. L. 2007, ApJ, 668, 806 BarrenaET2009
- Markevitch, M., Gonzalez, A. H., Clowe, D., et al. 2004, ApJ, 606, 819
- Markevitch, M., Gonzalez, A. H., David, L., et al. 2002, ApJ, 567, L27
- Markevitch, M., & Vikhlinin, A., 2007, Phys. Rep., 443, 1
- Massardi, M., Ekers, R. D., Ellis, S. C., & Maughan, B. 2010, ApJ, 718, L23
- Mastropietro, C., & Burkert, A. 2008, MNRAS, 389, 967
- Medzinski, E., Umetsu, K., Okabe, N., et al. 2016, ApJ, 817, 24
- Menanteau, F., et al. 2012, ApJ, 748, 7
- Merten, J., Coe, D., Dupke, R., et al. 2011, MNRAS, 417, 333
- Mitchell, N. L., McCarthy, I. G., Bower, R. G., Theuns, T., & Crain, R. A. 2009, MNRAS, 395, 180
- Molnar, S. M., 2015, *Cosmology with Clusters of Galaxies*, Nova Science Publishers, New York
- Molnar, S. 2016, Front. Astron. Space Sci., 2, 7
- Molnar, S. M., & Broadhurst, T. 2017, ApJ, 841, 46
- Molnar, S. M., & Broadhurst, T. 2015, ApJ, 800, 37
- Molnar, S. M., Broadhurst, T., Umetsu, K., et al. 2013, ApJ, 774, 70
- Molnar, S. M., Chiu, I.-N. T., Broadhurst, T., & Stadel, J. G. 2013, ApJ, 779, 63
- Molnar, S. M., Hearn, N. C., & Stadel, J. G. 2012, ApJ, 748, 45
- Molnar, S. M., et al. 2010, ApJ, 723, 1272
- Mroczkowski, T., Dicker, S., Sayers, J., et al. 2012, ApJ, 761, 47
- Okabe, N., Bourdin, H., Mazzotta, P., & Maurogordato, S. 2011, ApJ, 741, 116
- Navarro, J. F., Frenk, C. S., & White, S. D. M. 1997, ApJ, 490, 493
- Ng, K. Y., Dawson, W. A., Wittman, D., et al. 2015, MNRAS, 453, 1531
- Owers, M. S., Randall, S. W., Nulsen, P. E. J., et al., 2011, ApJ, 728, 27
- Ragozzine, B., Clowe, D., Markevitch, M., Gonzalez, A. H., & Bradač, M. 2012, ApJ, 744, 94
- Ricker, P. M. 2008, ApJS, 176, 293
- Sayers, J., Mroczkowski, T., Zemcov, M., et al. 2013, ApJ, 778, 52
- Springel, V., & Farrar, G. R. 2007, MNRAS, 380, 911
- Stroe, A., Harwood, J. J., Hardcastle, M. J., & Röttgering, H. J. A. 2014, MNRAS, 445, 1213
- Thompson, R., Davé, R., & Nagamine, K. 2015, MNRAS, 452, 3030
- Thompson, R., & Nagamine, K. 2012, MNRAS, 419, 3560
- van Weeren, R. J., Brügggen, M., Röttgering, H. J. A., & Hoefl, M. 2011, MNRAS, 418, 230
- van Weeren, R. J., Hoefl, M., Röttgering, H. J. A., et al. 2011, A&A, 528, A38
- van Weeren, R. J., Röttgering, H. J. A., Brügggen, M., & Hoefl, M. 2010, Science, 330, 347
- Watson, W. A., Iliev, I. T., Diego, J. M., et al. 2014, MNRAS, 437, 3776
- Zhang, C., Yu, Q., & Lu, Y. 2015, ApJ, 813, 129
- Zitrin, A., Zheng, W., Broadhurst, T., et al. 2014, ApJ, 793, L12